

Inertial Active Matter with Coulomb Friction

Alexander P. Antonov^{1,*}, Lorenzo Caprini^{2,†}, Anton Ldov¹, Christian Scholz¹, and Hartmut Löwen¹

¹*Institut für Theoretische Physik II: Weiche Materie, Heinrich-Heine-Universität Düsseldorf, Universitätsstrasse 1, D-40225 Düsseldorf, Germany*

²*Physics Department, University of Rome La Sapienza, Piazzale Aldo Moro 5, IT-00185 Rome, Italy*

 (Received 9 April 2024; revised 17 July 2024; accepted 4 October 2024; published 8 November 2024)

Friction is central to the motion of active (self-propelled) objects such as bacteria, animals, and robots. While in a viscous fluid friction is described by Stokes's law, objects in contact with other solid bodies are often governed by more complex empirical friction laws. Here, we study active particles subject to Coulomb friction using a combination of active granular experiments and simulations, supported by theoretical predictions. The interplay of friction and activity forces induces a rich behavior resulting in three distinct dynamical regimes. While for low activity Brownian motion is recovered, for large activity we observe a dynamical stop and go regime that continuously switches from diffusion and accelerated motion. For greater activity, we observe a supermobile dynamical regime characterized by a fully accelerated motion which is described by an anomalous scaling of the diffusion coefficient with the activity. These findings cannot be observed with Stokes viscous forces typical of active swimmers but are central in dry active objects.

DOI: [10.1103/PhysRevLett.133.198301](https://doi.org/10.1103/PhysRevLett.133.198301)

Friction [1] has been studied by using empirical models starting with pioneering observations that date back to 350 A.D. (Themistius): “It is easier to further the motion of a moving body than to move a body at rest.” This qualitative discovery was systematically investigated by Coulomb in 1785, who noted that dry friction force depends only on the velocity direction. He developed the celebrated Coulomb's friction law [2], which has proven to be fundamental on the macroscopic level [3,4]. At the molecular level, a further step in the study of dry friction was taken by de Gennes and Hayakawa, who independently explored its properties for Brownian motion [5,6] and suggested experimental realizations [7]. This research has prompted further theoretical [8–11] and experimental investigations in the context of passive granular particles [12,13], Brownian motors [14–17], and the piston problem [18,19].

Here, we study active particles governed by Coulomb friction whose motion is self-sustained by an activity, i.e., a nonequilibrium driving force with a stochastic evolution [20–22]. Thereby, the active particles continuously inject energy into the system, which is partially transformed into motion (kinetic energy) and partially irreversibly dissipated into the environment due to friction [23,24]. For wet systems [25,26] such as active colloids and bacteria, the friction is typically linear in the velocity [27,28] due to the liquid solvent originating from Stokes's law [29]. By

contrast, in dry systems such as robots and active granular particles [30–37], friction is generated by contact with the ground. In this case, dynamics are governed by Coulomb friction which is almost insensitive to velocity [5,6,28].

Using a combination of experiments and simulations, we showcase intriguing phenomena without counterparts in systems governed by Stokes friction. By increasing the activity, the particle switches from the standard Brownian motion dominated by white noise to a different dynamical “stop and go” regime [Figs. 1(b) and 1(c)] which alternates diffusive behavior to running, accelerated motion. Greater activity values induce an additional dynamical regime where the particle uniquely moves with an accelerated “supermobile” motion [Figs. 1(d) and 1(e)].

An active particle with Coulomb friction is experimentally realized via a vibrobot [39], which is activated by a vertically vibrating plate [Fig. 1(a)] attached to an electromagnetic shaker with frequency ν and amplitude A [see the Supplemental Material (SM) for details [38]]. These granular particles exhibit activity due to their asymmetric design [44]: the collisions between the particle legs and the plate lead to two-dimensional directed motion, with the typical speed growing as the shaker amplitude increases. Intuitively, the dynamics of this macroscopic object are governed by Coulomb friction, which is characterized by two components: a dynamic one which decelerates an object already in motion and a static one which impedes the motion. The dynamic part does not depend on velocity, while the static part contributes for vanishing velocity v , which hinders the motion of a stationary object. The friction force is thus determined by two friction coefficients

*Contact author: alexander.antonov@hhu.de

†Contact author: lorenzo.caprini@uniroma1.it

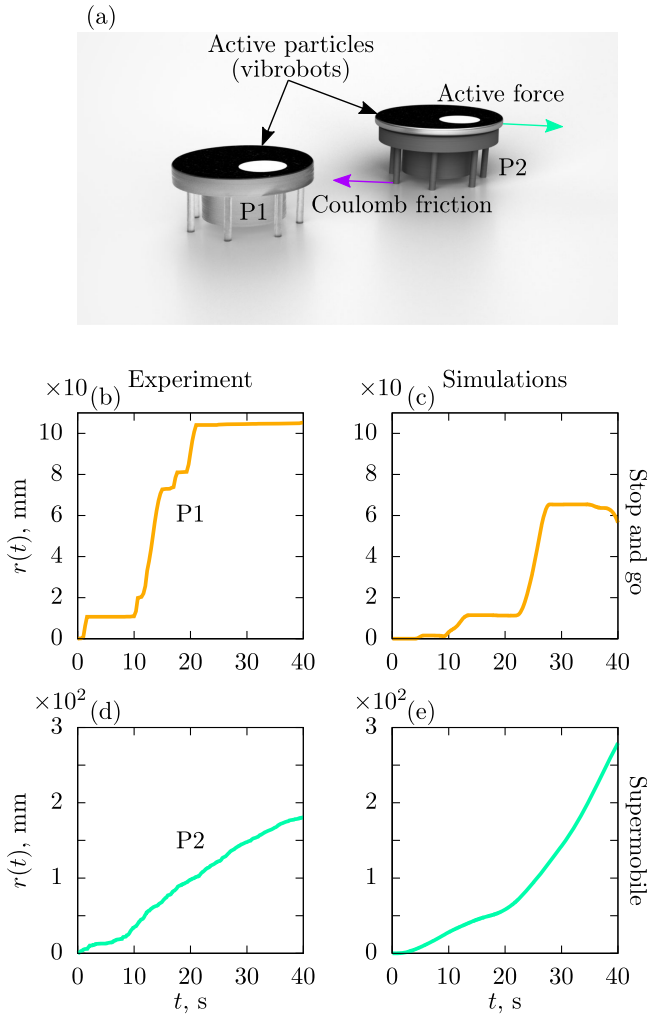


FIG. 1. Coulomb friction-induced anomalous dynamical states. (a) Illustration of the experimental setup: two active vibrobots (P1 and P2; see the SM for details [38]) governed by Coulomb friction. (b)–(e) Particle trajectories (radial coordinate) for different activities from (b),(d) experiments and (c),(e) simulations. The stop and go and supermobile regimes are obtained in experiments at shaker amplitudes $A = 9.381 \pm 0.046$ and 12.825 ± 0.089 μm , and in simulations at activity $f_0 = 1, 10$. The experiments are obtained at shaker frequency $\nu = 150$ Hz. The other simulation parameters are $\tau_0 = 100$, $\Delta_0 = 0$, and $v_0 = 0.1$.

which intrinsically depend on the material properties and are different for static and dynamic cases. The friction force $\sigma(\mathbf{v})$ can be described using the two-dimensional Tustin empirical model [45]:

$$\sigma(\mathbf{v}) = \Delta_C \hat{\mathbf{v}} \left[1 + \frac{\Delta_S - \Delta_C}{\Delta_C} e^{-(|\mathbf{v}|/v_s)} \right], \quad (1)$$

where $\Delta_{C,S}$ are the Coulomb dynamic and static friction coefficients, respectively, with $\Delta_S \geq \Delta_C$. Here, $\hat{\mathbf{v}} = \mathbf{v}/|\mathbf{v}|$ is the normalized velocity vector, which is equal to zero when $|\mathbf{v}| = 0$. The term v_s is the Stribeck velocity that sets the

sharpness of $\sigma(v)$ for $v \rightarrow 0$ [46]. Expression (1) provides a minimal description for studying dynamic and static Coulomb friction in the equation of motion. Previously, theoretical analysis focused mainly on the simpler dynamical friction case $\Delta_C = \Delta_S$, where Eq. (1) reduces to $\sigma(\mathbf{v}) = \Delta_C \hat{\mathbf{v}}$, or $\sigma(v) = \Delta_C \text{sgn}(v)$ in one dimension. In particular, in de Gennes's and Hayakawa's papers, emphasis was placed on velocity autocorrelation [5] and steady-state distribution [6], while Touchette *et al.* provided the exact solution [8]. More recently, the role of colored noise on the velocity distribution was unveiled in the case of weak memory [47]. Compared to [47], we focus on large activity and discover anomalous dynamical regimes that were not previously observed.

The dynamics of an active particle in two dimensions with mass m and dry friction is minimally modeled as a Langevin equation for the particle velocity $\mathbf{v} = \dot{\mathbf{r}}$,

$$m\dot{\mathbf{v}}(t) = -\sigma(\mathbf{v}(t)) + \sqrt{2K}\xi(t) + \mathbf{n}(t)f, \quad (2)$$

where $\xi(t)$ is Gaussian white noise with unit variance and K determines the noise strength. The active force is represented by the term $\mathbf{n}(t)f$, where f is the activity. The term $\mathbf{n}(t)$ is an Ornstein-Uhlenbeck process with autocorrelation time τ and dynamics

$$\dot{\mathbf{n}}(t) = -\frac{\mathbf{n}(t)}{\tau} + \sqrt{\frac{2}{\tau}}\boldsymbol{\eta}(t), \quad (3)$$

where $\boldsymbol{\eta}(t)$ is Gaussian white noise with zero average and unit variance. This active force choice corresponds to the active Ornstein-Uhlenbeck particle dynamics [48–55].

In what follows, we use Δ_C , $\sqrt{\tau K}/\Delta_C$, and $\tau K/m\Delta_C$ as units of force, time, and length, respectively. With this choice, the system is characterized by four dimensionless parameters (see the SM for details [38]): the reduced activity $f_0 = f/\Delta_C$, which quantifies the active force effect compared to friction; the reduced noise strength $1/\tau_0 = \sqrt{K/\tau}/\Delta_C$, which determines the impact of the noise kicks on the particle evolution; two friction parameters, i.e., the relative magnitude of the static and dynamic friction force $\Delta_0 = \Delta_S/\Delta_C - 1$ and the rescaled Stribeck velocity $v_0 = mv_s/\sqrt{\tau K}$. We set $v_0 = 0.1$ since static friction has to affect the dynamics only for a small velocity, and a low noise strength $1/\tau_0 = 10^{-2}$, as usual in active matter experiments.

For small shaker amplitudes, i.e., small activity, the active force $\mathbf{n}(t)f_0$ cannot exceed the friction force value on average, and thus its dynamic effect is suppressed. The resulting motion is similar to the one shown by standard Brownian particles. Indeed, intuitively, the active force induces an effective dry friction coefficient which is smaller (larger) than Δ_C if the active force and the velocity have the same (opposite) sign. Therefore, the characteristic trajectory of this Coulomb-governed Brownian dynamical state

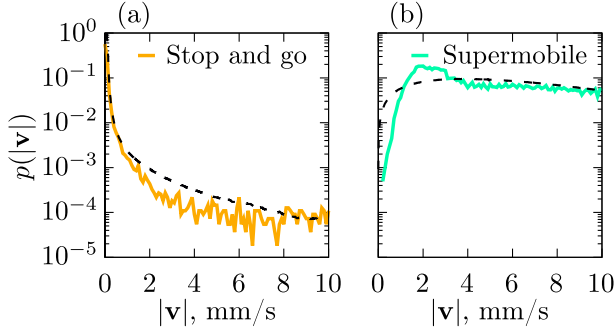


FIG. 2. Velocity distribution $p(|\mathbf{v}|)$ calculated from experiments (solid lines) and simulations (dashed lines). (a) The stop and go regime from experiments with shaker amplitude $A = 9.381 \pm 0.046 \mu\text{m}$ and from simulations with activity $f_0 = 0.3$. (b) The supermobile regime observed at $A = 12.825 \pm 0.089 \mu\text{m}$ and $f_0 = 4.5$. In (a) and (b) the shaker frequency is $\nu = 150 \text{ Hz}$, while the other parameters are $\tau_0 = 100$, $v_0 = 0.1$, and $\Delta_0 = 0$.

is not qualitatively different from the usual regime displayed by a Brownian particle. Here, as in the passive case, static friction cannot keep the particle stationary for an arbitrary time [5]. In the experimental setup, the velocity in this Brownian regime is so small that it falls below the resolution limit. However, its behavior can be robustly demonstrated through simulations (see the SM [38]).

As the shaker amplitude (and thus the activity f_0) is increased, the active force $\mathbf{n}(t)f_0$ is more likely to exceed the friction force value in some time interval. When this happens, the trajectory displays fast acceleration (here the particle “goes”). These regimes are suppressed when, by fluctuations, the active force is smaller than the Coulomb

friction: when this happens, the particle behaves as a Brownian particle, as observed for small f_0 , i.e., the particle “stops.” Here, the particle is not really stuck but rather slow compared to the “go” state. This stop and go behavior can be directly observed in the particle trajectory in experiments [Fig. 1(b) and Movie 1 in the SM [38]] and simulations [Fig. 1(c)]. A further increase of the shaker amplitude and f_0 allows the active force to permanently exceed the friction value, except for the small time window when a spatial component of $\mathbf{n}(t)f_0$ reverses its direction. In this state, the friction mechanism cannot hinder the motion except for in these small time windows. This induces a different regime characterized by supermobile behavior, where the particle continuously accelerates and suddenly decelerates. [See Fig. 1(d) or Movie 2 in the SM [38] for experiments and Fig. 1(e) for simulations.] The difference between the dynamical regimes emerges in the steady-state distribution $p(|\mathbf{v}|)$ of the velocity modulus. Indeed, in the stop and go regime, $p(|\mathbf{v}|)$ is peaked at zero [Fig. 2(a)] because the particle spends a long time moving slowly. By contrast, in the supermobile regime, $p(|\mathbf{v}|)$ displays a bump at a large speed before slowly decaying to zero [Fig. 2(b)].

In the mechanism discussed here, dimensions are not crucial (see the SM [38]). Therefore, we systematically study the dynamics (2) and (3) in one dimension that, in addition, we can treat analytically. These three dynamical states can be characterized by investigating the long-time diffusion coefficient D_L extracted from the mean squared displacement (MSD) $\langle [x(t) - x(0)]^2 \rangle$. Independently of the activity and Coulomb friction coefficients, this observable shows a small-time ballistic regime $\langle [x(t) - x(0)]^2 \rangle \sim t^2$

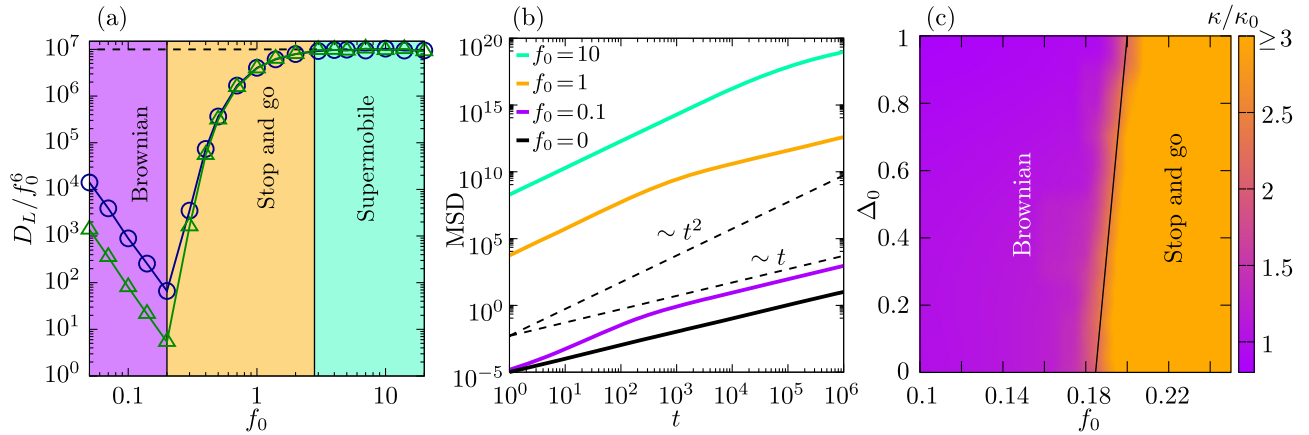


FIG. 3. Stop and go and supermobile states. (a) Long-time time diffusion coefficient D_L rescaled by f_0^6 as a function of f_0 , with $\Delta_0 = 0$ (blue circles) and $\Delta_0 = 1$ (green triangles). The parameter region corresponding to the Brownian, stop and go, and supermobile regimes are displayed in violet, yellow, and green, respectively, while the transitions are marked with vertical lines. (b) Mean squared displacement $\text{MSD} = \langle (x(t) - x(0))^2 \rangle$, as a function of time t for different values of f_0 in the three dynamical states with $\Delta_0 = 0$. Dashed black lines denote the ballistic and diffusive timescales. The colors have the same ordering as the MSD profiles. (c) State diagram in the plane of activity f_0 and relative friction coefficient Δ_0 . The color gradient shows the smoothed excess kurtosis, normalized with the value for the passive system. The solid black line is a guide for the eye and indicates the crossover from Brownian and stop and go regimes. The other parameters of the simulations are $v_0 = 0.1$ and $\tau_0 = 100$.

[Fig. 3(a)], which is purely induced by the activity, as usual for active particles [56,57]. In the long-time regime, the MSD approaches a diffusive behavior $\sim t$, which is due to the random change of the active force direction present in all of the dynamical states. From here, we can extract the long-time diffusion coefficient D_L that is reported as a function of f_0 for vanishing ($\Delta_0 = 0$) and nonvanishing static frictions ($\Delta_0 > 0$). For small values of f_0 corresponding to the Brownian regime, D_L scales as f_0^2 , as expected for standard active Brownian particles (see the SM for a scaling argument [38]). When the stop and go regime is approached, D_L starts increasing faster with f_0 . This anomalous scaling is due to the go regimes, which allows the particle to further explore the surrounding space. When stop events are suppressed because of the large f_0 value, a scaling $D_L \sim f_0^6$ is reached in correspondence with the supermobile state [Fig. 3(a)]. We remark that the system switches from different dynamical states (f_0 scaling) via smooth crossover regimes.

The relative amplitude of static and dynamic friction Δ_0 affects the diffusion properties only in the Brownian regime by decreasing D_L , while it leaves the stop and go and supermobile states almost unchanged. This is because static friction plays a negligible role compared to dynamical friction during a go state since $|v| \gg v_0$, and thus $\sigma(v) \approx \Delta_C \text{sgn}(v)$. However, we intuitively expect that an increase of the static friction, via Δ_0 , could affect the transition line from the Brownian to the stop and go regime. To further characterize the role of Δ_0 , we focus on the steady-state velocity properties. Indeed, during go states the velocity gains large values, which is represented by the long tails of the velocity distribution and which we quantify by studying its fourth moment. Specifically, we focus on the excess kurtosis, i.e., the deviation of the fourth velocity moment from the Gaussian value, $\kappa = \langle v^4 \rangle / \langle v^2 \rangle^2 - 3$. We normalize this observable with the excess kurtosis κ_0 at zero activity ($f_0 = 0$) so that κ/κ_0 reads ≈ 1 in the Brownian regime and assumes values $\gg 1$ in the stop and go state. Our analysis as a function of f_0 and Δ_0 [Fig. 3(c)] reveals that static friction $\Delta_0 > 0$ hinders the transition to the stop and go regime. Indeed, in this case, the active force needs to exceed a larger total dry friction to induce acceleration.

To further shed light on the effect of activity f_0 and static friction Δ_0 , we numerically and theoretically analyze the velocity distribution $p(v)$. As we expect from the kurtosis analysis, this observable does not show remarkable differences between the Brownian regime and the purely passive case ($f_0 = 0$), where $p(v)$ decays exponentially as $\propto e^{-\tau_0|v|}$. By resorting to path-integral techniques [43] (see the SM for details [38]), the expression for $p(v)$ can be generalized for small activity $f_0 \ll 1$ (Brownian state), where the main contribution occurs for $|v| \ll 1$ and reads

$$p(v) \propto e^{-\tau_0[|v|(\Delta_0+1) - \Delta_0/2v_0v^2 - f_0^2|v|^3/4(\Delta_0+1) + \mathcal{O}(v^4)]}. \quad (4)$$

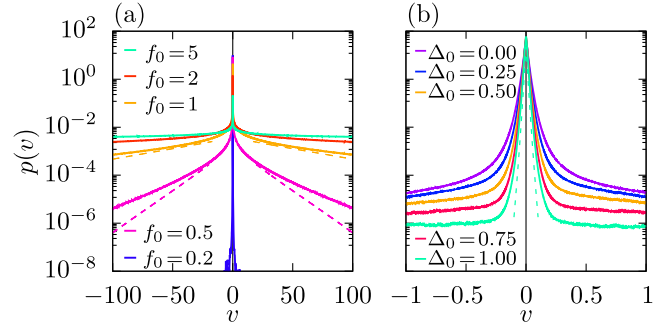


FIG. 4. Probability distributions. (a) Velocity probability distribution $p(v)$ for $\Delta_0 = 0$ for various f_0 . (b) $p(v)$ for $f = 0.25$ for various Δ_0 . The dashed lines in (a) correspond to the analytical prediction (5), and the dashed lines in (b) correspond to the analytical prediction (4) up to the first order. The colors have the same ordering as the density profiles. The other parameters of the simulations are $v_0 = 0.1$ and $\tau_0 = 100$.

Here, static friction and activity have roughly the same effect, providing small deviations from the exponential tails [Figs. 4(a) and 4(b)]. Static friction, however, plays a pivotal role in vanishing velocities [Fig. 4(b)]. By contrast, in the stop and go state for larger values of f_0 , the full shape of the distribution is distorted [Fig. 4(a)]. In particular, in the stop and go regime, the tails slowly decay to zero, while in the supermobile state the distribution is nearly flat, with a small peak for vanishing velocity. Remarkably, our method is able to also provide an analytical approximation for the velocity distribution $p(v)$ for large activity f_0 , where typically $|v| \gg 1$,

$$p(v) \propto e^{-(n_f^2/2)}. \quad (5a)$$

Here, n_f is set implicitly via the equation

$$2\tau_0[n_f f_0 - \ln(n_f f_0) - 1] = v, \quad n_f > \frac{1}{f_0}. \quad (5b)$$

Equation (5) holds in the absence of static friction $\Delta_0 = 0$, while the full expression for $\Delta_0 > 0$ is reported in the SM [38]. However, in agreement with the previous analysis, static friction provides a negligible contribution on $p(v)$ for $|v| \gg 1$.

Our theoretical approach allows us to predict the typical escape particle trajectory by expressing v as a function of n for vanishing noise (see the SM for details [38]):

$$\frac{dv}{dn} = \mp \frac{\text{sgn}(v)\tau_0}{n} [1 + \Delta_0 e^{-(|v|/v_0)}] \pm f_0 \tau_0. \quad (6)$$

The two solutions imply that the particle displays a hysteresislike trajectory in the (n, v) plane [Fig. 5(a)]. The particle, initially placed at $v = 0$ and $n = 0$, maintains zero velocity until the active force exceeds the friction, i.e., at the threshold value such that $|v| = n f_0 = 1$. From here,

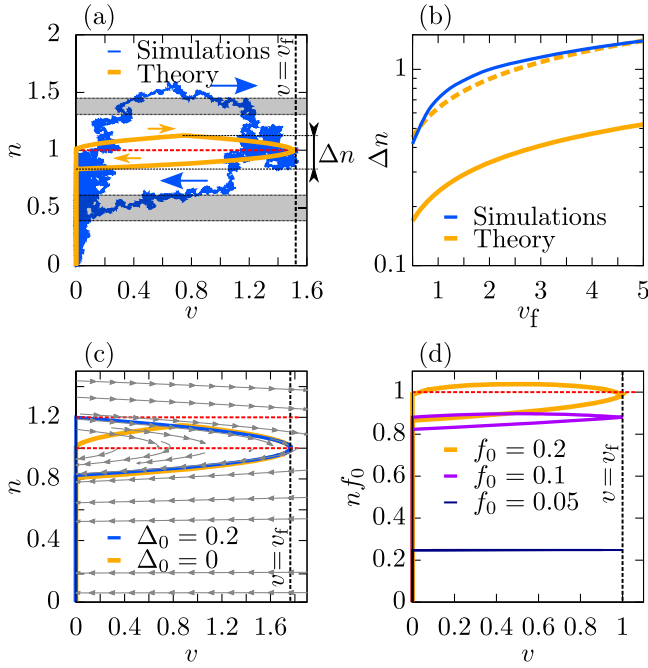


FIG. 5. Analytical approach. (a),(c),(d): Escape-and-return particle trajectory in the plane of v and n . (a) Is obtained for the maximum velocity $v_f = 1.5$ (vertical dashed line). It reports a single trajectory from numerical simulations (blue line) and from the integration of Eq. (6) (orange line). Variances of average maximum (minimum) activity during the escape (return) n_f (n_a) are shown as gray rectangles. (c) Cases $\Delta_0 = 0$ (without static friction) and $\Delta_0 = 0.2$ (with static friction) at $v_f \approx 1.77$ (vertical dashed line). (d) Deterministic trajectories for $f_0 = 0.05, 0.1$, and 0.2 exploring active Brownian and stop and go regimes. The curves are obtained via the numerical minimization of Eq. (S17) (see the SM [38]) at $v_f = 1$ (vertical line). In (a), (c), and (d), the horizontal red lines correspond to the threshold activity levels $n = 1/(f_0 + \Delta_0)$. (b) Loop height Δn for various v_f , defined as the difference between maximum and minimum activity in the loop. The theoretical predictions (solid orange line) are compared with the numerical results obtained by averaging over 200 trajectories (blue line). By adjusting an *ad hoc* multiplicative factor that is omitted in Eq. (5a), we show that the exponential behavior of the prediction (dashed orange line) quantitatively matches the simulations. (c) Analytical escape trajectories for the different static frictions $\Delta_0 = 0$ (orange line) and $\Delta_0 = 0.2$ (blue line) and the same maximum velocity $v_f \approx 1.77$ (vertical dashed line). The other parameters are $f_0 = 1$, $\Delta_0 = 0$, $v_0 = 0.1$, and $\tau_0 = 100$.

the particle starts accelerating [the upper sign in Eq. (6)] and reaches a maximum velocity when the activity decreases below the threshold value. At this point, the particle slows down and relaxes to its initial state [the lower sign in Eq. (6)]. This hysteresislike trajectory is a visualization of the stop and go regime and is purely induced by dry friction. Indeed, this behavior cannot be achieved by active dynamics governed by Stokes viscous forces for which $v \propto n$ or in the Brownian regime (small f_0) where the hysteresis degenerates into a back-and-forth line [Fig. 5(d)]. The hysteresis height loop, Δn is more pronounced when

higher velocities v_f are reached during the escape [Fig. 5(b)]. In addition, this height is increased by static friction, as shown by the escape trajectories in Fig. 5(c). This is because the go state is hindered by the static friction, unlike in the case $\Delta_0 = 0$.

The emergence of the three dynamic states due to the interplay between activity and Coulomb friction suggests their existence in a broader range of experimental systems beyond the considered system. Good candidates are Hexbug particles [58–62] or sliding robots [63], where Coulomb friction can be enhanced by modifying the material properties or propulsion mechanism. Alternatively, activity can be induced on any granular object via programmed shakers that produced colored noise [44,64–66]. The emerging stop and go and supermobile regimes could lead to unprecedented collective phenomena for active systems ranging from giant density fluctuations to pulsating clusters. In addition, our findings can pave the way toward the development of intriguing applications in active granular matter: supermobile active granulates could be employed for efficient spatial exploration and food search by taking advantage of their enhanced diffusivity. Furthermore, while we have provided experimental realizations of stop and go and supermobile regimes, further miniaturization and higher resolution techniques are required to investigate the Brownian regime. A relevant example that fulfills these needs and shares similarities with the vibrobot setup is dust mitigation through vibrating surfaces [67].

Acknowledgments—A. P. A., A. L., C. S., and H. L. acknowledge the financial support by Deutsche Forschungsgemeinschaft (German Research Foundation) Project No. LO 418/25-1. L. C. acknowledges the European Union MSCA-IF fellowship for funding the project CHIAGRAM.

- [1] A. Fall, B. Weber, M. Pakpour, N. Lenoir, N. Shahidzadeh, J. Fiscina, C. Wagner, and D. Bonn, *Phys. Rev. Lett.* **112**, 175502 (2014).
- [2] C. A. Coulomb, *Théorie des Machines Simples en Ayant Égard au Frottement de Leurs Parties et à la Roideur des Cordages* (Bachelier, Paris, 1821).
- [3] H. Olsson, K. J. Åström, C. C. De Wit, M. Gäfvert, and P. Lischinsky, *Eur. J. Control* **4**, 176 (1998).
- [4] E. Pennestrì, V. Rossi, P. Salvini, and P. P. Valentini, *Nonlinear Dyn.* **83**, 1785 (2016).
- [5] P.-G. de Gennes, *J. Stat. Phys.* **119**, 953 (2005).
- [6] H. Hayakawa, *Physica (Amsterdam)* **205D**, 48 (2005).
- [7] S. Daniel, M. K. Chaudhury, and P.-G. de Gennes, *Langmuir* **21**, 4240 (2005).
- [8] H. Touchette, E. V. der Straeten, and W. Just, *J. Phys. A* **43**, 445002 (2010).
- [9] Y. Chen and W. Just, *Phys. Rev. E* **89**, 022103 (2014).
- [10] T. Lequy and A. M. Menzel, *Phys. Rev. E* **108**, 064606 (2023).
- [11] A. Plati, A. Puglisi, and A. Sarracino, *J. Phys. A* **57**, 155001 (2024).

- [12] A. Gnoli, A. Puglisi, and H. Touchette, *Europhys. Lett.* **102**, 14002 (2013).
- [13] A. Lemaître, C. Mondal, I. Procaccia, and S. Roy, *Phys. Rev. B* **103**, 054110 (2021).
- [14] A. Baule and P. Sollich, *Europhys. Lett.* **97**, 20001 (2012).
- [15] Y. Chen and W. Just, *Phys. Rev. E* **90**, 042102 (2014).
- [16] A. Manacorda, A. Puglisi, and A. Sarracino, *Commun. Theor. Phys.* **62**, 505 (2014).
- [17] M. Semeraro, G. Gonnella, E. Lippiello, and A. Sarracino, *Symmetry* **15**, 200 (2023).
- [18] A. Sarracino, A. Gnoli, and A. Puglisi, *Phys. Rev. E* **87**, 040101(R) (2013).
- [19] T. G. Sano and H. Hayakawa, *Phys. Rev. E* **89**, 032104 (2014).
- [20] M. C. Marchetti, J. F. Joanny, S. Ramaswamy, T. B. Liverpool, J. Prost, M. Rao, and R. A. Simha, *Rev. Mod. Phys.* **85**, 1143 (2013).
- [21] J. Elgeti, R. G. Winkler, and G. Gompper, *Rep. Prog. Phys.* **78**, 056601 (2015).
- [22] C. Bechinger, R. Di Leonardo, H. Löwen, C. Reichhardt, G. Volpe, and G. Volpe, *Rev. Mod. Phys.* **88**, 045006 (2016).
- [23] J. O’Byrne, Y. Kafri, J. Tailleur, and F. van Wijland, *Nat. Rev. Phys.* **4**, 167 (2022).
- [24] É. Fodor, R. L. Jack, and M. E. Cates, *Annu. Rev. Condens. Matter Phys.* **13**, 215 (2021).
- [25] A. Zöttl and H. Stark, *J. Phys. Condens. Matter* **28**, 253001 (2016).
- [26] H. Löwen, *J. Chem. Phys.* **152**, 040901 (2020).
- [27] P. Romanczuk and L. Schimansky-Geier, *Phys. Rev. Lett.* **106**, 230601 (2011).
- [28] P. Romanczuk, M. Bär, W. Ebeling, B. Lindner, and L. Schimansky-Geier, *Eur. Phys. J. Special Topics* **202**, 1 (2012).
- [29] J. Elgeti, R. G. Winkler, and G. Gompper, *Rep. Prog. Phys.* **78**, 056601 (2015).
- [30] I. S. Aranson, D. Volfson, and L. S. Tsimring, *Phys. Rev. E* **75**, 051301 (2007).
- [31] A. Kudrolli, G. Lumay, D. Volfson, and L. S. Tsimring, *Phys. Rev. Lett.* **100**, 058001 (2008).
- [32] N. Kumar, H. Soni, S. Ramaswamy, and A. Sood, *Nat. Commun.* **5**, 4688 (2014).
- [33] N. Koumakis, A. Gnoli, C. Maggi, A. Puglisi, and R. Di Leonardo, *New J. Phys.* **18**, 113046 (2016).
- [34] M. Agrawal and S. C. Glotzer, *Proc. Natl. Acad. Sci. U.S.A.* **117**, 8700 (2020).
- [35] L. Walsh, C. G. Wagner, S. Schlossberg, C. Olson, A. Baskaran, and N. Menon, *Soft Matter* **13**, 8964 (2017).
- [36] P. Baconnier, D. Shohat, C. H. López, C. Coulais, V. Démery, G. Düring, and O. Dauchot, *Nat. Phys.* **18**, 1234 (2022).
- [37] L. Caprini, D. Breoni, A. Ldov, C. Scholz, and H. Löwen, *Commun. Phys.* **7**, 343 (2024).
- [38] See Supplemental Material at <http://link.aps.org/supplemental/10.1103/PhysRevLett.133.198301>, which includes Refs. [39–43], for experimental setup and analytical calculations.
- [39] C. Scholz, S. Jahanshahi, A. Ldov, and H. Löwen, *Nat. Commun.* **9**, 5156 (2018).
- [40] V. P. Maslov and M. V. Fedoriuk, *Semiclassical Approximation in Quantum Mechanics* (Reidel, Dordrecht, 1981).
- [41] A. Antonov, A. Leonidov, and A. Semenov, *Phys. Rev. E* **108**, 024134 (2023).
- [42] L. D. Landau and E. M. Lifshitz, *Mechanics: Vol. 1* (Butterworth-Heinemann, London, 1976).
- [43] B. Caroli, C. Caroli, and B. Roulet, *J. Stat. Phys.* **26**, 83 (1981).
- [44] L. Caprini, A. Ldov, R. K. Gupta, H. Ellenberg, R. Wittmann, H. Löwen, and C. Scholz, *Commun. Phys.* **7**, 52 (2024).
- [45] L. Marton and B. Lantos, *IEEE Trans. Ind. Electron.* **54**, 511 (2007).
- [46] R. Stribeck, *Z. Ver. Dtsch. Ing.* **46**, 1341 (1902).
- [47] P. M. Geffert and W. Just, *Phys. Rev. E* **95**, 062111 (2017).
- [48] G. Szamel, *Phys. Rev. E* **90**, 012111 (2014).
- [49] C. Maggi, M. Paoluzzi, N. Pellicciotta, A. Lepore, L. Angelani, and R. Di Leonardo, *Phys. Rev. Lett.* **113**, 238303 (2014).
- [50] R. Wittmann, C. Maggi, A. Sharma, A. Scacchi, J. M. Brader, and U. M. B. Marconi, *J. Stat. Mech.* (2017) 113207.
- [51] L. Caprini and U. M. B. Marconi, *Soft Matter* **14**, 9044 (2018).
- [52] Y. Fily, *J. Chem. Phys.* **150**, 174906 (2019).
- [53] E. Woillez, Y. Kafri, and N. S. Gov, *Phys. Rev. Lett.* **124**, 118002 (2020).
- [54] D. Martin, J. O’Byrne, M. E. Cates, É. Fodor, C. Nardini, J. Tailleur, and F. Van Wijland, *Phys. Rev. E* **103**, 032607 (2021).
- [55] Y.-E. Keta, R. L. Jack, and L. Berthier, *Phys. Rev. Lett.* **129**, 048002 (2022).
- [56] B. ten Hagen, S. van Teeffelen, and H. Löwen, *J. Phys. Condens. Matter* **23**, 194119 (2011).
- [57] L. Caprini and U. Marini Bettolo Marconi, *J. Chem. Phys.* **154**, 024902 (2021).
- [58] O. Dauchot and V. Démery, *Phys. Rev. Lett.* **122**, 068002 (2019).
- [59] C. Tapia-Ignacio, L. L. Gutierrez-Martinez, and M. Sandoval, *J. Stat. Mech.* (2021) 053404.
- [60] M. Leoni, M. Paoluzzi, S. Eldeen, A. Estrada, L. Nguyen, M. Alexandrescu, K. Sherb, and W. W. Ahmed, *Phys. Rev. Res.* **2**, 043299 (2020).
- [61] D. Horvath, C. Slabý, Z. Tomori, A. Hovan, P. Miskovsky, and G. Bánó, *Phys. Rev. E* **107**, 024603 (2023).
- [62] L. Chen, K. J. Welch, P. Leishangthem, D. Ghosh, B. Zhang, T.-P. Sun, J. Klukas, Z. Tu, X. Cheng, and X. Xu, [arXiv:2302.10525](https://arxiv.org/abs/2302.10525).
- [63] P. Hamon, M. Gautier, and P. Garrec, in *Proceedings of the 2010 IEEE/RSJ International Conference on Intelligent Robots and Systems, Taipei, 2010* (IEEE, New York, 2010), pp. 6187–6193.
- [64] A. Kudrolli, *Phys. Rev. Lett.* **104**, 088001 (2010).
- [65] J. Designe, O. Dauchot, and H. Chaté, *Phys. Rev. Lett.* **105**, 098001 (2010).
- [66] H. Soni, N. Kumar, J. Nambisan, R. K. Gupta, A. Sood, and S. Ramaswamy, *Soft Matter* **16**, 7210 (2020).
- [67] A. A. Abubakar, B. S. Yilbas, H. Al-Qahtani, A. Alzaydi, and S. Alhelou, *Sci. Rep.* **10**, 14346 (2020).